Advances in Science and Technology Research Journal

Advances in Science and Technology Research Journal 2022, 16(1), 85–94
https://doi.org/10.12913/22998624/143051
ISSN 2299-8624, License CC-BY 4.0

Received: 2021.08.21
Accepted: 2021.12.10
Published: 2022.01.01

Path Interval and Its Relevance to Cutting Force in Ball and Filleted End Milling

Tsutomu Sekine[1*]

[1] Department of Systems Design Engineering, Faculty of Science and Technology, Seikei University, Japan
E-mail: ts_s@outlook.com

ABSTRACT

Computerized milling process is widely used in product manufacturing. Although manufacturing has gradually become highly-automated, the selection of machining conditions still remains an ever-present challenge in the process. To provide some findings contributable for the process planning, this study focuses on ball and filleted end milling. After brief explanations were given to the path interval determinations in both milling processes, the experiments were conducted to verify and characterize each procedure. The results of computational procedures showed good agreement with the experimental ones. Then, material removal rate and cutting force were analytically proposed for effective selection of machining conditions. The following findings were obtained from the demonstrations with discussion. Ball end milling required relatively large cutting force in the first tool path even though the material removal rate was comparatively small. On the contrary, filleted end mill enabled us to maintain a moderate cutting force in the first tool path even if the material removal rate expanded with increasing tool radius.

Keywords: path interval, material removal rate, cutting force, ball end mill, filleted end mill.

INTRODUCTION

Computer numerical control (CNC) machine tool with digital twin technology is starting to become increasingly common all over the world. The development is rapidly progressing through integrating and combining the elemental technologies such as intelligent control, health management, and so on [1, 2]. Tool management using digital twin technology is also attracting attention to improve manufacturing efficiency and machined surface feature [3, 4]. Performance optimization is one of the objectives in digital twin, and selecting the optimal machining conditions is primarily of importance in practical production. Process planning is commonly implemented through computer-aided manufacturing to create manufacturing process information essential for operating a machine tool [5, 6]. CNC milling process is being widely used as one of the core manufacturing technologies [7]. Tool path generation can provide manufacturing process information for a milling process, whereas there are a variety of the machining parameters affecting surface quality, machining accuracy, manufacturing efficiency, and so on [8–11].

Path interval is known as one of the setting conditions in tool path generation. The determination has focused mainly on the relationship between manufacturing efficiency and machined surface feature. The related studies mainly focuses on a typical tool geometry such as ball, flat, or filleted end mill. In ball end milling, the path interval can be calculated based on an intersection problem between a designed shape and a cutting edge of ball end mill in a machining state [12–15]. In flat and filleted end milling, there are the two kinds of procedures available to determine a proper path interval [16–24]. The one employs a two dimensional procedure considering a cutter profile on an imaginary section introduced geometrically, and the other is a three dimensional computation based on a geometrical modeling of milling process. The related

research findings have been recently provided from various perspectives [25–27]. Moreover, the comparative study with two or more tool geometries has been scarcely made to select a proper machining condition.

In the last three decades, a variety of contributions were also made to reveal the importance of cutting force with the development of methodologies, techniques, and instruments. Yang and Park analyzed a cutting geometry of ball-end mill with plane rake faces [28]. After that, the instantaneous cutting force was predicted using the cutting force model based on the analyses. Lee and Altintaş proposed a prediction method of cutting force in ball end milling [29]. Orthogonal cutting data were used to determine cutting force coefficients in the prediction. Budak and Ozlu developed a thermomechanical cutting process model. Then, they provided the relationship between cutting force and feedrate in ball end milling [30]. Wojciechowski et al. proposed cutting force model including variable edge forces, and the experiments were made to investigate the influence of surface inclination angle on edge forces' values [31]. Meanwhile, material removal rate (MRR) has been also studied as one of the interesting factors in milling. Park et al. described a feedrate optimization entailing the calculation of cutting force from MRR [32]. Quintana et al. reported experimental results to clarify the relationships between surface roughness and MRR in ball end milling [33]. However, it would be difficult to search the study focusing on the relevance to path interval. At any rate, author has been unaware of it so far.

The objective of this study is to investigate the relationships between machining factors and path interval determination in end milling. This study focuses particularly on cutting force in ball and filleted end milling. Geometrical analyses will be demonstrated to calculate MRR and cutting force in the machining processes. Then, the comparisons and discussion will be made to provide the practical findings for effective tool selection. Finally, conclusion will be drawn from the experimental and numerical evidences.

Path interval determination

Path interval determinations in both ball and filleted end milling will be theoretically described in this section. To verify the theoretical expressions, the experiments were performed after the preliminary examinations of machining conditions. Hereafter, assuming, for simplicity, that milling process is performed on a plane. In addition, the tool diameters were selected from the commonly-used sizes of both end mills having two straight cutting edges. Ball end milling was examined without tool inclination, whereas filleted end milling was investigated with tool inclination. The unit of tool inclination angle is expressed as deg. to aid an intuitive understanding.

The theoretical calculation in ball end milling

A cross-feed distance between adjacent tool paths can be expressed by path interval. This study uses $L/2$ as a path interval, so that $L/2$ denotes a unilateral distance from a tool center point to a section assumed situationally to measure scallop height h. Figure 1 illustrates a geometrical relationship regarding path interval determination in ball end milling. Given that ball end mill with tip radius R moves along a trajectory of the tool center point to create a designed shape and h is predetermined, $L/2$ is given as follows:

$$\frac{L}{2} = \sqrt{2Rh - h^2} \tag{1}$$

This path interval determination refers to [14, 15]. The path interval is achievable through solving an intersection problem on an instantaneous section. Tool inclination angle does not affect path interval determination since the tool tip geometry of ball end mill is a hemisphere projected onto the assumed section.

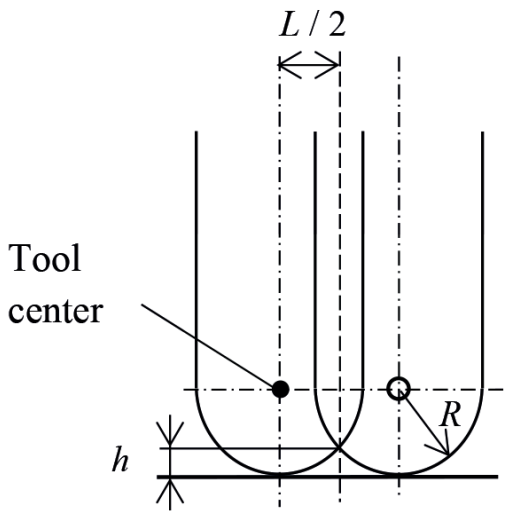

Fig. 1. A geometrical relationship between $L/2$ and h in ball end milling

The computational procedure in filleted end milling

A path interval determination in filleted end milling was recently proposed as one of the remarkable algorithms [24]. This study employed the approach. The algorithm covers that filleted end milling with a tool inclination is performed along a tool feed direction and on a plane to create a designed surface. Figure 2 is provided to display several radii, i.e. R, R_b, and R_{cr}, of filleted end mill with a tool inclination along a tool feed direction. Moreover, the figure shows a tool inclination angle θ. A torus is theoretically introduced to express the geometrical features of cutting edge geometry. In reference [21], the step-by-step procedure was reported in detail. After $L/2$ is properly determined using the procedure with iterative calculations, the summation of adjacent path intervals $L/2$ can provide total path interval L.

Experiments

Some experiments with CNC milling machine, PSF550-CNC, were made to verify the theoretical and computational approaches mentioned above. The general view is shown in Figure 3. The spindle can mechanistically adjust tool inclination angle θ in accordance with each experimental condition, and the tilting range is available from -30 to 90 deg. The tilting mechanism was used in filleted end milling. End mills were individually attached to the milling machine's spindle in each experiment, and each radius R of both tools was 5.0, 6.0, and 7.0 mm. Each corner radius R_{cr} in filleted end milling was 1.0, 2.0, and 3.0 mm. Ball end mills (2BE) and filleted end mills (2RBE) were made by FUKUDA SEIKO Co., Ltd. A synthetic wood, SANMODUR MH-E, was used as a material to be machined. A vice attached to the machine's table, and the workpiece was clamped by the vice before each experiment.

Table 1 shows milling conditions in each ball end mill. For your reference, tool number 1, 2 and 3 correspond to BM1, BM2, and BM3, respectively. In addition, these tool radius were 5.0, 6.0, and 7.0 mm from the smallest tool number. Conditions BM1a and BM1b have difference in scallop height set as 0.05 and 0.10 mm. BM2a, BM2b, BM3a, and BM3b were also designed in the same manner. Note that ball end milling was performed without tool inclination. In contrast, Table 2 displays milling conditions in each filleted end mill. In the name of each condition, FM means filleted end milling when tool inclination angle θ = 5 deg., and the conditions were designed in accordance with the similar manner to the ones in ball end milling. The experimental conditions were determined after the results were reviewed in preliminary investigations.

Figure 4 illustrates scanning-line tool paths from one direction. Path interval $L/2$ was determined computationally and the trajectory of tool path was prepared a priori under the

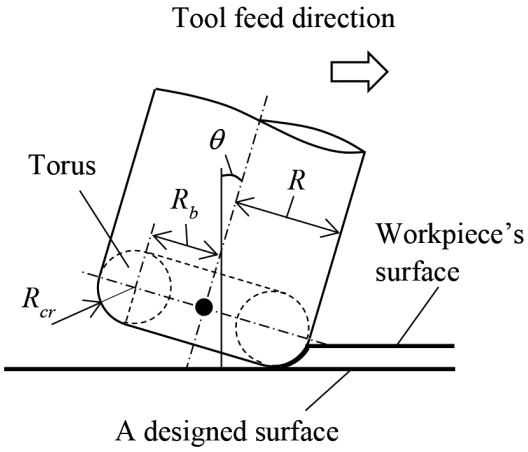

Fig. 2. Several radii and a tool inclination angle θ in filleted end milling

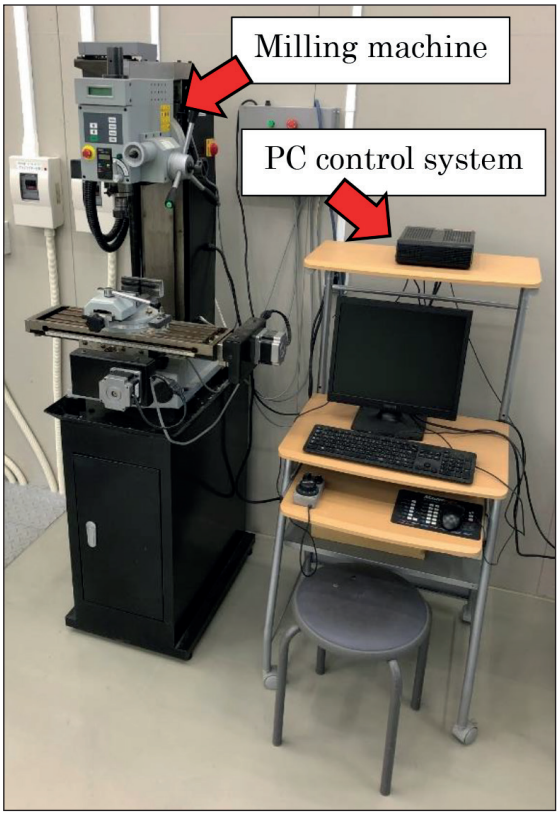

Fig. 3. A general view of CNC milling machine

Table 1. Experimental conditions in ball end milling

Parameters	BM1a	BM1b	BM2a	BM2a	BM3a	BM3b
Tool radius *R* [mm]	5.0	5.0	6.0	6.0	7.0	7.0
Tool rotational speed S [min^{-1}]	1200	1200	1200	1200	1200	1200
Feed rate *f* [mm/min]	100	100	100	100	100	100
Scallop height *h* [mm]	0.050	0.100	0.050	0.100	0.050	0.100
Path interval *L*/2 [mm]	0.705	0.995	0.773	1.091	0.835	1.179

Table 2. Experimental conditions in filleted end milling

Parameters	FM1a	FM1b	FM2a	FM2b	FM3a	FM3b
Tool radius *R* [mm]	5.0	5.0	6.0	6.0	7.0	7.0
Tool tip R_{cr} [mm]	1.0	1.0	2.0	2.0	3.0	3.0
Tool rotational speed *S* [min^{-1}]	1200	1200	1200	1200	1200	1200
Feed rate *f* [mm/min]	100	100	100	100	100	100
Scallop height *h* [mm]	0.050	0.100	0.050	0.100	0.050	0.100
Path interval L / 2 [mm}	2.090	2.843	2.115	2.884	2.140	2.924

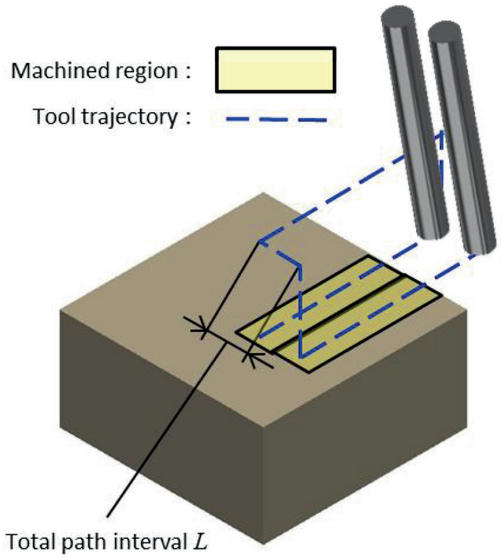

Fig. 4. A schematic example of tool path and machined region in each experiment

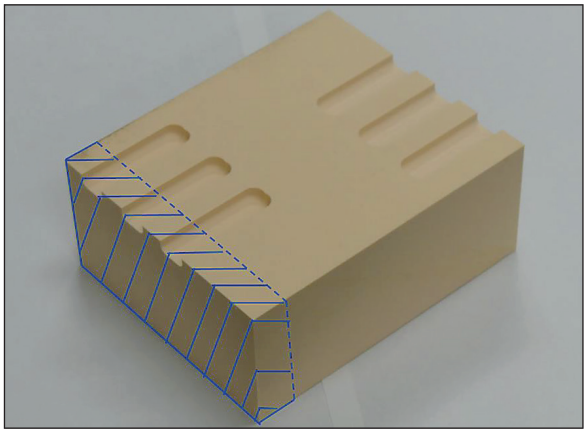

Fig. 5. A machined material and cut-out part (shaded area)

condition that scallop height *h* was set as 0.05 and 0.10 mm. The milling processes in each experimental condition were performed three times to investigate the repeatability of machined surface feature.

A specimen was cut out after the experiments, and the scallop height was measured based on the observation of the cut-out specimen. Shaded area in Figure 5 represents a cut-out part from a machined material. Optical microscope (Mitutoyo TM-505) was used for the measurements after experiments. The cut-out specimen was placed on the stage of microscope. Then, the scallop height was measured based on the digital image observed by optical microscope. The measurements were made three times in connection with the number of experiments. The comparisons were made with the theoretical and experimental results.

RESULTS AND VERIFICATION

The graphical representations in Figures 6 and 7 are experimental results in ball and filleted end milling. In both figures, the *x* axis on the graphs indicates tool radii used in experiments. The *y* axis on the graph also represents scallop height *h* [mm]. Each white bar graph with error

bar indicates the average scallop height calculated from three experimental results in each condition. In contrast, each green bar graph represents the computational value obtained using the above formula or procedure in each condition. These evidences represented that computational values showed good agreement with experimental values. The differences between experimental and computational values were within plus or minus 0.05 mm at most. It means that the theoretical and computational approaches used in this study have remarkable potential for accurate estimations in each path interval determination. Even if the filleted end mill with different corner radius was used in each experiment, the computational approach was available to provide predicted values with high accuracy. Tables 1 and 2 also indicated that filleted end mill enabled us to set more than twice the path interval, compared with the one in the corresponding radius of ball end mill. This tendency was not the same in all condition, and a little differences were found in each condition. The increasing rate enlarged as the corner radius decreased in filleted end mill. When a scallop height was set to double value in the same kind of tool, the path intervals were given as about 1.4 times the values in ball end milling. Each ratio of path interval expressed similar tendency in filleted end milling even though there were differences with practically considerable amount in precision processing. In all comparable cases, the ratios in filleted end milling were slightly smaller than the ones in ball end milling.

Material removal rate and cutting force

This section deals with MRR and cutting force in end milling. It is widely accepted that cutting force has direct influence on tool life [34]. Accordingly, the careful thought is inevitably required in determining machining conditions. The geometrical analyses will be provided based on the findings obtained previously in the related study [27]. Note that the demonstrations are targeted at one cutting edge during one rotation of a tool. It is difficult to exactly calculate an uncut chip geometry in an instantaneous machining state, whereas the geometrical calculation can be approximated to grasp several characteristics of MRR and cutting force in milling process. This study employed the practicable, cost-effective calculation of cutting force in end milling.

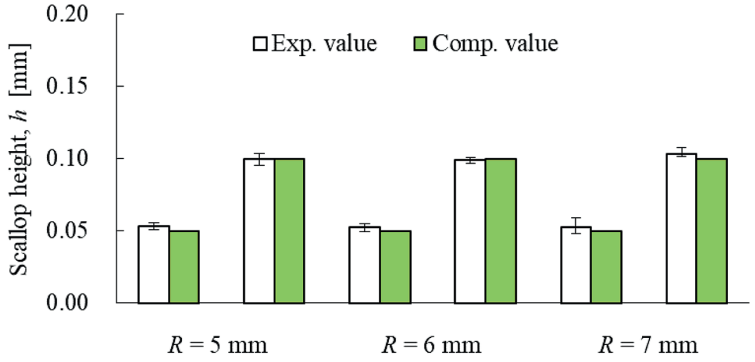

Fig. 6. Experimental verification of path interval determination in ball end milling

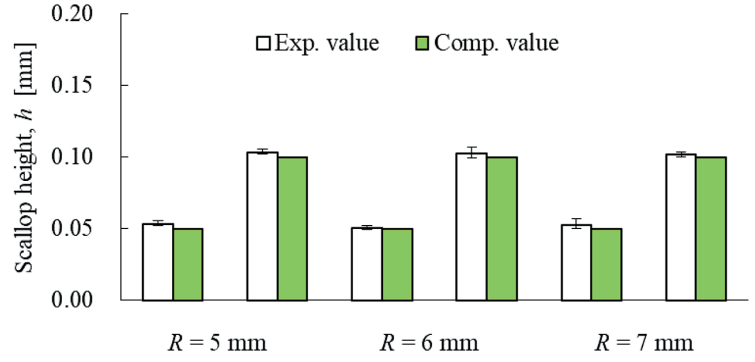

Fig. 7. Experimental verification of path interval determination in filleted end milling

Geometrical analyses

The variables in Figure 8 are individually specified to estimate cutting force from the calculation of *MRR* in ball end milling. In the following part of this section, we separately deal with the first tool path and the subsequent ones in feed direction. For the sake of clarity, path number is added to all variables used below. In the strict sense, the number in parenthesis indicates path number, and the number 2 means the second tool path or above. From the drawing, α_{tz} and R_{tz} are given as follows:

$$\alpha_{tz}(1) = \frac{R - ap}{R} \tag{2}$$

$$R_{tz}(1) = R\cos\alpha_{tz} \tag{3}$$

Then, an area of section with reference to cutting region A_s and a material removal rate *MRR* are provided in the following formulas:

$$A_s(1) = \frac{R^2(\eta_{tz} - \sin\eta_{tz})}{2} \tag{4}$$

$$MRR(1) = \frac{A_s(1)f}{60000} \tag{5}$$

where: η_{tz} is an angle calculated by $\sin^{-1}(R_{tz}(1)/R)$,
f is a federate.

Note that the unit of $MRR(1)$ is cm^3/s since unit conversion is included in equation (5). A spindle power for manufacturing operation can be obtained using *MRR*:

$$P_c(1) = K_m MRR(1) \tag{6}$$

where: K_m is a material constant depending on cutting condition, tool geometry, and workpiece's material, and so on.

The value is commonly determined either by experiments or from related handbooks such as reference [35]. This study set 0.20 kWs/cm^3 as the value converted by using a manufacturer's value [36] based on ASTM D2240 test. A cutting torque T_s can be calculated as follows:

$$T_s(1) = \frac{60000P_c}{2\pi S} \tag{7}$$

where: S is a spindle speed in milling process.

A tangential cutting force at a cutting edge F_t can be estimated after the calculation:

$$F_t(1) = \frac{1000T_s}{R_{tz}} \tag{8}$$

From empirical modeling and experiments, the thrust cutting force F_{th} is given as $F_t/2$ [32]. As a result, a cutting force at a cutting edge F_r can be expressed as the resultant of F_t and F_{th}:

$$F_r(1) = \sqrt{F_t^2 + F_{th}^2} \tag{9}$$

In the second path or above, depth of cut *ap* is substituted by scallop height *h* in the half machining region. Hence, the following formulas can calculate the values of α_{tz}:

$$\alpha_{tz}(2) = \frac{R - h}{R} \tag{10}$$

Equation (3) can be similarly used to calculate $R_{tz}(2)$. η_{tz} is also obtainable using $R_{tz}(2)$. As shown in Figure 9, the calculation of an area with reference to cutting region is rather complicated in the second path or above. In the drawing, we would like to get the area inside thick line to calculate $MRR(2)$. As the first step, $A_s(2)$ can be derived with the consideration of area related to scallop height A_{sh} and removal part in arched area A_{rm}:

$$A_s(2) = A_s(1) - 2A_{rm} \tag{11}$$

$$A_{rm} = \frac{A_s(1)}{2} - \left(A_{sh} + R_{tz}(2)(ap - h)\right) \tag{12}$$

Then, equations (5) to (9) enable us to calculate $MRR(2)$ and $F_r(2)$ in the same manner.

On the other hand, filleted end milling with the variables related to the calculation of *MRR* and cutting force is shown in Figure 10. To begin with, l_a and l_b are necessary for the subsequent calculations:

$$l_a(1) = (R_{cr} - ap)\cos\theta \tag{13}$$

$$l_b(1) = (R_{cr} - ap)\sin\theta \tag{14}$$

Then, α_{tz} and R_{tz} can be obtained using l_a and l_b:

$$\alpha_{tz}(1) = \sin^{-1}\left(\frac{l_a}{R_{cr}}\right) \tag{15}$$

$$R_{tz}(1) = R_{cr}\cos\alpha_{tz} \tag{16}$$

In this case, η_{tz} can be calculated as follows:

$$\eta_{tz}(1) = \sin^{-1}\left(\frac{R_b + l_b(1)}{R_b + R_{tz}(1)}\right) \tag{17}$$

The profile of torus's section becomes a multi-order curve complicated to treat an area of section with reference to cutting region $A_s(1)$. To arrange the complexity, it is geometrically reasonable to express the area as a half ellipse.

In preparation for the calculation, a major radius of half ellipse $R_{ea}(1)$ equals $(R_b + R_{tz}(1))\sinh_{tz}(1)$, and a minor radius of half ellipse $R_{eb}(1)$ corresponds to h. Accordingly,

$$A_s(1) = \frac{\pi R_{ea}(1) R_{eb}(1)}{2} \tag{18}$$

After that, the calculation of $MRR(1)$ can be obtained from equation (5). Furthermore, $P_c(1)$ and $T_s(1)$ can be calculated through equations (6) and (7). A tangential cutting force at a cutting edge $F_t(1)$ in filleted end milling is given as follows:

$$F_t(1) = \frac{1000 T_s}{R_b + R_{tz}} \tag{19}$$

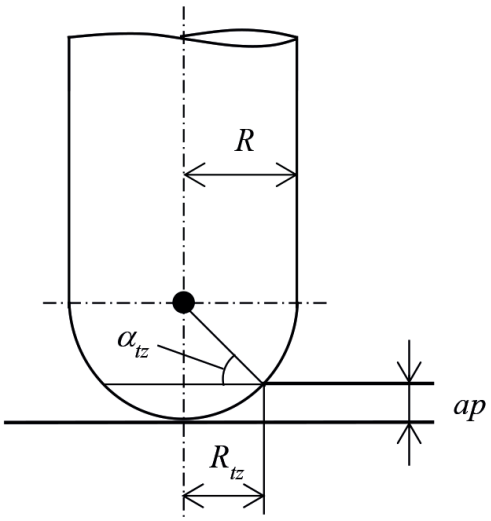

Fig. 8. The variables related to calculating MRR and cutting force in ball end milling

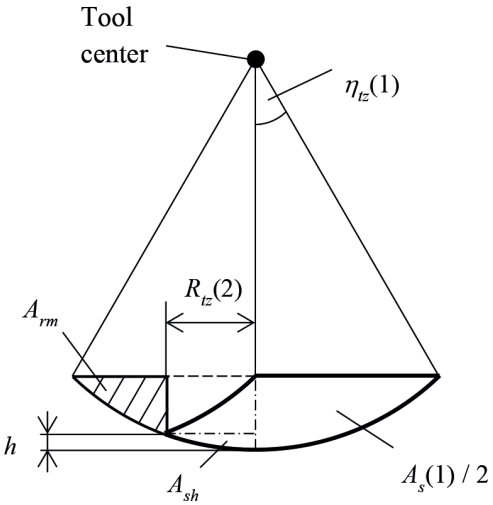

Fig. 9. Several areas of section with reference to cutting region in the second path or above

Then, $F_r(1)$ can be achieved through equations (9) since the calculation of F_{th} in ball end milling is similarly applicable in filleted end milling.

In the second path or above, depth of cut ap is substituted by scallop height h in the calculations of equations (13) and (14). Then, $\alpha_{tz}(2)$, $R_{tz}(2)$, and $\eta_{tz}(2)$ can be obtained using equations (15) to (17). For the elliptic approximation, we can apply the same manner as the calculations of $R_{ea}(1)$ and $R_{eb}(1)$. Although the calculation of a removal part in arched area A_{rm} inevitably faces mathematical complexity, the following formula can express the area under the approximation:

$$A_{rm} = R_{ea}(1) R_{eb}(1) \left(\cos^{-1}\left(1 - \frac{w_h}{R_{ea}(1)}\right) - \left(1 - \frac{w_h}{R_{ea}(1)}\right) \sqrt{\frac{2w_h}{R_{ea}(1)} - \frac{w_h^2}{R_{ea}(1)^2}} \right) \tag{20}$$

where: w_h is $R_{ea}(1) - R_{ea}(2)$.

Equation (11) is similarly applicable to obtain $A_s(2)$. Finally, equations (5) to (9) are also available to calculate $MRR(2)$ and $F_r(2)$ in the same manner used for the first path. The theoretical analyses described above are widely applicable for a practical workpiece such as stainless steel.

DEMONSTRATIONS AND DISCUSSION

Material removal rate MRR and cutting force F_r were calculated as demonstrations based on the experimental conditions. The tool inclination

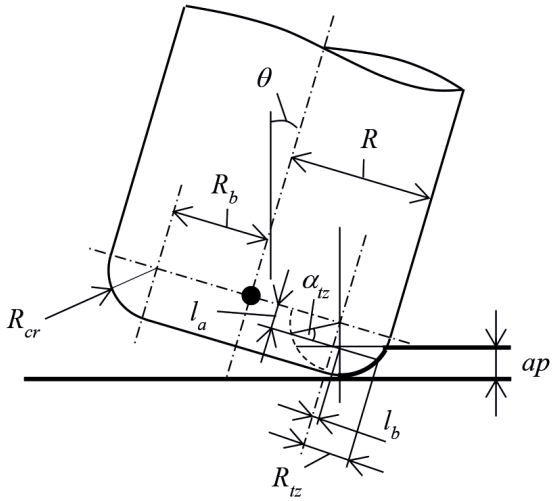

Fig. 10. The variables related to calculating MRR and cutting force in filleted end milling

Table 3. Material removal rates *MRR* and cutting forces F_r in ball end milling

Parameters	BM1a	BM1b	BM2a	BM2b	BM3a	BM3b
R [mm]	5.0	5.0	6.0	6.0	7.0	7.0
MRR(1) [cm^3/s]	0.00245	0.00245	0.00269	0.00269	0.00291	0.00291
MRR(2) [cm^3/s]	0.00113	0.00154	0.00124	0.00169	0.00134	0.00183
F_r(1) [N]	2.00	2.00	1.99	1.99	1.99	1.99
F_r(2) [N]	0.93	1.26	0.92	1.25	0.92	1.25

Table 4. Material removal rates *MRR* and cutting forces F_r in filleted end milling

Parameters	FM1a	FM1b	FM2a	FM2b	FM3a	FM3b
R [mm]	5.0	5.0	6.0	6.0	7.0	7.0
R_{cr} [mm]	1.0	1.0	2.0	2.0	3.0	3.0
MRR(1) [cm^3/s]	0.00355	0.00355	0.00441	0.00441	0.00497	0.00497
MRR(2) [cm^3/s]	0.00225	0.00271	0.00260	0.00320	0.00281	0.00351
F_r(1) [N]	1.30	1.30	1.47	1.47	1.56	1.56
F_r(2) [N]	0.82	0.99	0.87	1.07	0.88	1.10

angle θ was set to 5.0 deg. in filleted end milling. Depth of cut *ap* was also set to a half of 1.0 mm in all conditions. The numerical representations in Tables 3 and 4 are the results of demonstrations. From the numerical evidences, *MRR* increased with increasing tool radius. The increasing rate of *MRR* became lower with increasing corner radius in filleted end milling. Moreover, each value of *MRR* in ball end mill was smaller than the corresponding one in filleted end mill. The difference expanded more and more with increasing the tool radius. Here, the focus is given to the ratios of *MRR*(2). They can be rewritten using the conditions as follows: BM1b / BM1a, BM2b / BM2a, and BM3b / BM3a in ball end milling; moreover, FM1b / FM1a, FM2b / FM2a, and FM3b / FM3a in filleted end milling. The ratios of *MRR*(2) in ball end milling are 1.357, 1.358, and 1.359, respectively. In contrast, the ratios of *MRR*(2) in filleted end milling are 1.204, 1.231, and 1.249, respectively. From the numerical values, the increasing rate of *MRR*(2) with increasing *h* was almost unchanged in ball end milling. In filleted end milling, the rate slightly increased unlike the results of ball end milling. The values of increasing rate with increasing *h* in ball end milling were larger than the ones in filleted end milling, whereas *MRR*(2) in filleted end mill was more than double the value, compared with the one in the corresponding radius of ball end mill.

The next attention was drawn to cutting force F_r. The variations of F_r were different in the tool tip geometry of end mill. The slight decrease was observed in ball end milling. In contrast, the gradual increase was found in filleted end milling. Each value of F_r in ball end mill was larger than the corresponding one in filleted end mill. The cause of this result was considered to be the difference in tool tip geometry. From the result, filleted end mill would possess this advantage revealed in this study even if machining condition is changed variously. The difference of corresponding values in two tables reduced gradually with increasing the tool radius. As the next step, we would like to consider the ratios of F_r(2) in the same manner as the ones of *MRR*(2). The ratios of F_r(2) in ball and filleted end milling showed absolute agreement with the ones of *MRR*(2). From the numerical results, The ratios of F_r(2) can be estimated based on the rate of *MRR*(2). It was evident in ball end milling that relatively large cutting force was required in the first tool path even though *MRR* was comparatively small. On the contrary, the results indicated that filleted end mill enabled us to maintain a moderate cutting force F_r in the first tool path even if *MRR* expanded with increasing tool radius. These findings would imply that filleted end mill makes it possible to achieve stable milling process and long tool life even if *MRR* increases according to the variation of machining state.

CONCLUSION

This study describes the comparisons of path interval determinations in ball and filleted end milling. Material removal rate and cutting force were also investigated to grasp the relevance to

path interval. After path interval determinations were explained briefly, the characteristics of each procedure were revealed with experimental verifications. The results of computational procedures showed good agreement with the experimental ones. Then, material removal rate *MRR* and cutting force F_r were proposed based on geometrical analyses. Some formulas were explained to calculate the two parameters, and the demonstrations were made under each machining condition. As a results, the following findings were obtained from the theoretical analyses: (i) each value of *MRR* in ball end mill was smaller than the corresponding one in filleted end mill. The difference expanded more and more with increasing the tool radius. (ii) The values of increasing rate with increasing *h* in ball end milling were larger than the ones in filleted end milling, whereas *MRR*(2) in filleted end mill was more than double the value, compared with the one in the corresponding radius of ball end mill. (iii) In the first tool path, relatively large cutting force was required in ball end milling even though the *MRR* was comparatively small. On the contrary, filleted end mill enabled us to maintain a moderate cutting force in the first tool path even if the *MRR* expanded with increasing tool radius.

Acknowledgments

The authors would like to thank the financial support provided by OSG Fund, Shotoku Science Foundation, and the research grant from Faculty of Science and Technology, Seikei University.

REFERENCES

1. Armendia M., Ghassempouri M., Ozturk E., Peysson F. Twin-Control: A Digital Twin Approach to Improve Machine Tools Lifecycle. Springer; 2019.
2. Armendia M., Peysson F., Euhus D. Twin-Control: A New Concept Towards Machine Tool Health Management. In Proc. of 3rd European Conference of the Prognostics and Health Management Society, Bilbao, Spain 2016. https://doi.org/10.36001/phme.2016.v3i1.1584
3. Christiand, Kiswanto G. Digital Twin Approach for Tool Wear Monitoring of Micro-Milling. Procedia CIRP. 2020; 93: 1532–1537.
4. Sekine T. Study on Tool Condition Parameters Intended for Smart Tool Management in Filleted end Milling. Advances in Science and Technology Research Journal. 2021; 15: 108–116.
5. Al-wswasi M., Ivanov A., Makatsoris H. A survey on smart automated computer-aided process planning (ACAPP) techniques. The International Journal of Advanced Manufacturing Technology. 2018; 97: 809–832.
6. Nguyen T.K., Phung L.X., Bui N.T. Novel Integration of CAPP in a G-Code Generation Module Using Macro Programming for CNC Application. Machines. 2020; 8: 61–76.
7. Mali R.A., Gupta T.V.K., Ramkumar J. A comprehensive review of free-form surface milling– Advances over a decade. Journal of Manufacturing Processes. 2021; 62: 132–167.
8. Liang F., Kang C., Fang F. A review on tool orientation planning in multi-axis machining. International Journal of Production Research. 2020; 1–31.
9. Honeycutt A., Schmitz T.L. Milling Bifurcations: A Review of Literature and Experiment. Journal of Manufacturing Science and Engineering. 2018; 140: 120801.
10. Peng T., Xu X. Energy-efficient machining systems: a critical review. The International Journal of Advanced Manufacturing Technology. 2014; 72: 1389–1406.
11. Moradnazhad M., Unver H.O. Energy efficiency of machining operations: A review. Proceedings of the Institution of Mechanical Engineers Part B J. Eng. Manufacture. 2016; 231: 1871–1889.
12. Tuan L.H., Makhanov S.S. Accurate Scallop Evaluation Method Considering Kinematics of Five-axis Milling Machine for Ball-end Mill. Materials Science and Engineering. 2020; 840: 012006.
13. Xu J., Zhang H., Sun Y. Swept surface-based approach to simulating surface topography in ball-end CNC milling. The International Journal of Advanced Manufacturing Technology. 2018; 98: 107–118.
14. Sekine T., Obikawa T. Normal-Unit-Vector-Based Tool Path Generation Using a Modified Local Interpolation for Ball-End Milling. Journal of Advanced Mechanical Design, Systems, and Manufacturing. 2010; 4: 1246–1260.
15. Obikawa T., Sekine T. A Higher-Order Formula of Path Interval for Tool-Path Generation. International Journal of Automation Technology. 2011; 5: 663–668.
16. Liang F., Kang C., Lu Z., Fang F. Iso-scallop tool path planning for triangular mesh surfaces in multi-axis machining. Robotics and Computer-Integrated Manufacturing. 2021; 72: 102206.
17. Sekine T., Obikawa T. Novel path interval determination in 5-axis flat end milling. Applied Mathematical Modelling. 2015; 39: 3459–3480.
18. Zhang X., Zhang W., Zhang J., Pang B., Zhao W. Systematic study of the prediction methods for ma-

chined surface topography and form error during milling process with flat-end cutter. Proceedings of the Institution of Mechanical Engineers Part B. J. Eng. Manufacture. 2019; 233: 226–242.

19. Sekine T., Obikawa T., Hoshino M. Establishing a Novel Model for 5-Axis Milling with Filleted End Mill. Journal of Advanced Mechanical Design, Systems, and Manufacturing. 2012; 6: 296–309.
20. Bedi S., Ismail F., Mahjoob M.J., Chen Y. Toroidal Versus Ball Nose and Flat Bottom End Mills. International Journal of Advanced Manufacturing Technology. 1997; 13: 326–332.
21. Sekine T. A Computational Algorithm for Path Interval Determination in Multi-Axis Filleted End Milling. Advances in Science and Technology Research Journal. 2020; 14: 198–205.
22. Quinsat Y., Lavernhe S., Lartigue C. Characterization of 3D surface topography in 5-axis milling. Wear. 2011; 271: 590–595.
23. Hendriko H. A hybrid analytical and discrete based methodology to calculate path scallop of helical toroidal cutter in fiveaxis milling. FME Trans. 2018; 46: 552–559.
24. Sekine T., Kameya K. Remarkable characteristics of a novel path interval determination in filleted end milling. Journal Européen des Systèmes Automatisés. 2021; 54: 461–468.
25. Khorasani A.M., Yazdi M.R.S., Safizadeh M.S. Analysis of machining parameters effects on surface roughness: a review. International Journal of Computational Materials Science and Surface Engineering. 2012; 5: 68–84.
26. Habibi M., Kilic Z.M., Altintas Y. Minimizing Flute Engagement to Adjust Tool Orientation for Reducing Surface Errors in Five-Axis Ball End Milling Operations. Journal of Manufacturing Science and Engineering. 2021; 143: 021009.
27. Sekine T. Study on Tool Condition Parameters Intended for Smart Tool Management in Filleted End Milling. Advances in Science and Technology Research Journal. 2021; 15: 108–116.
28. Yang M., Park H. The prediction of cutting force in ball-end milling. International Journal of Machine Tools and Manufacture. 1991; 31: 45–54.
29. Lee P., Altintaş Y. Prediction of ball-end milling forces from orthogonal cutting data. International Journal of Machine Tools and Manufacture. 1996; 36: 1059–1072.
30. Budak E., Ozlu E. Development of a thermomechanical cutting process model for machining process simulations. CIRP Annals. 2008; 57: 97–100.
31. Wojciechowski S., Maruda R.W., Nieslony P., Krolczyk G.M. Investigation on the edge forces in ball end milling of inclined surfaces. International Journal of Mechanical Sciences. 2016; 119: 360–369.
32. Park H., Qi B., Dang D.V., Park D.Y. Development of smart machining system for optimizing feedrates to minimize machining time. Journal of Computational Design and Engineering. 2018; 5: 299–304.
33. Quintana G., de Ciurana J., Ribatallada J. Surface Roughness Generation and Material Removal Rate in Ball End Milling Operations. Materials and Manufacturing Processes. 2010; 25: 386–398.
34. Sousa V.F.C., Silva F.J.G., Fecheira J.S., Lopes H.M., Martinho R.P., Casais R.B., Ferreira L.P. Cutting Forces Assessment in CNC Machining Processes: A Critical Review. Sensors. 2020; 20: 4536.
35. Dynomax. Spindle component facts and engineering data. Part two. https://dynospindles.com/vault/technical/Book-of-Spindles-Part-2.pdf
36. Sanyo chemical industry Ltd. Synthetic Wood for Modeling & Tooling. https://www.sanyo-chemical.co.jp/eng/wp/wp-content/uploads/2021/04/PC_No.115.pdf